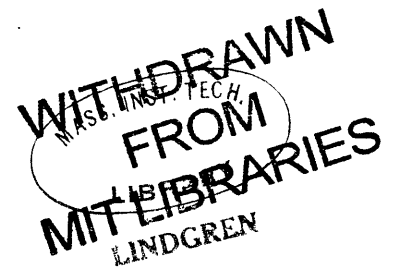ANALYSIS OF MESOSCALE FRONTOGENESIS

AND DEFORMATION FIELDS

by

R. THROOP BERGH

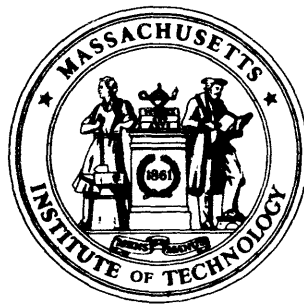B. S., Trinity College

(1960)

SUBMITTED IN PARTIAL FULFILLMENT OF THE

REQUIREMENTS FOR THE DEGREE OF

MASTER OF SCIENCE

AT THE

MASSACHUSETTS INSTITUTE OF TECHNOLOGY

May 1967

Signature of author................................
/ Department of Meteorology, May 1967.

Certified
          Thesis Supervisor

Accepted by.......................................
          Chairman, Departmental Committee on
                Graduate Students

ANALYSIS OF MESOSCALE FRONTOGENESIS

AND DEFORMATION FIELDS

by

R. Throop Bergh

ABSTRACT

Three cold fronts which pass through the N.S.S.L. Beta
Network are examined. The mesoscale deformation fields are
computed and are used to evaluate frontogenesis for each
case. In each case, deformation is found to be more impor-
tant than convergence in frontogenesis. On this scale,
cyclonic vorticity is found to be weakly correlated with
the fronts.

Two models are proposed to explain why no apparent
change in frontal intensity occurs, although huge rates
of frontogenesis are calculated. One is rejected on the
basis of the results, the other requires a balance between
mesoscale frontogenetical processes and turbulent fronto-
lytical processes.

In the final section, the relation between the wind-
shift and temperature break is studied. Large rates of
frontogenesis occur when these two events occur simul-
taneously. When the wind-shift outruns the temperature break,
sizeable rates of frontogenesis are still found, and the
mechanism responsible is investigated.

ACKNOWLEDGEMENTS

TABLE OF CONTENTS

Introduction

<u>Fronts</u>- The presence of frontal surfaces in the atmosphere has
been recognized for many years. The achievement of understand-
ing of this phenomenon, however, has been disappointingly slow.
During the early 1900's the air-mass concept was introduced in
Norway, synthesizing the earlier endeavors of such men as
Fitzroy, Shaw, and Lempfert. The name "front" was most likely
adopted because the battle between polar and tropical air-masses
was analagous to the lines of implingement of the great armies
facing each other in Europe at this time. A frontal zone arises
from the juxtaposition of two air-masses of different origin
brought to close proximity so as to form a zone of rapid tempera-
ture transition.

Classically, a boundary surface on which there is a dis-
continuity of a given element such as temperature is generally
called a frontal surface. When the variable shows a discon-
tinuity such as figure <u>1(a)</u>, it is said to have a discontinuity
of zero order. When the variable is continuous figure <u>1(b)</u>,but
its derivative is discontinuous across the surface, it has a
discontinuity of the first order and so on. The intersection
of this three dimensional surface with the ground is referred
to as a front. Real discontinuities do not exist in nature, so
the front so defined is somewhat of an idealization. However,
due to the scale of synoptic charts, frontal zones may appear as

(a)

(b)

T-2

T-1

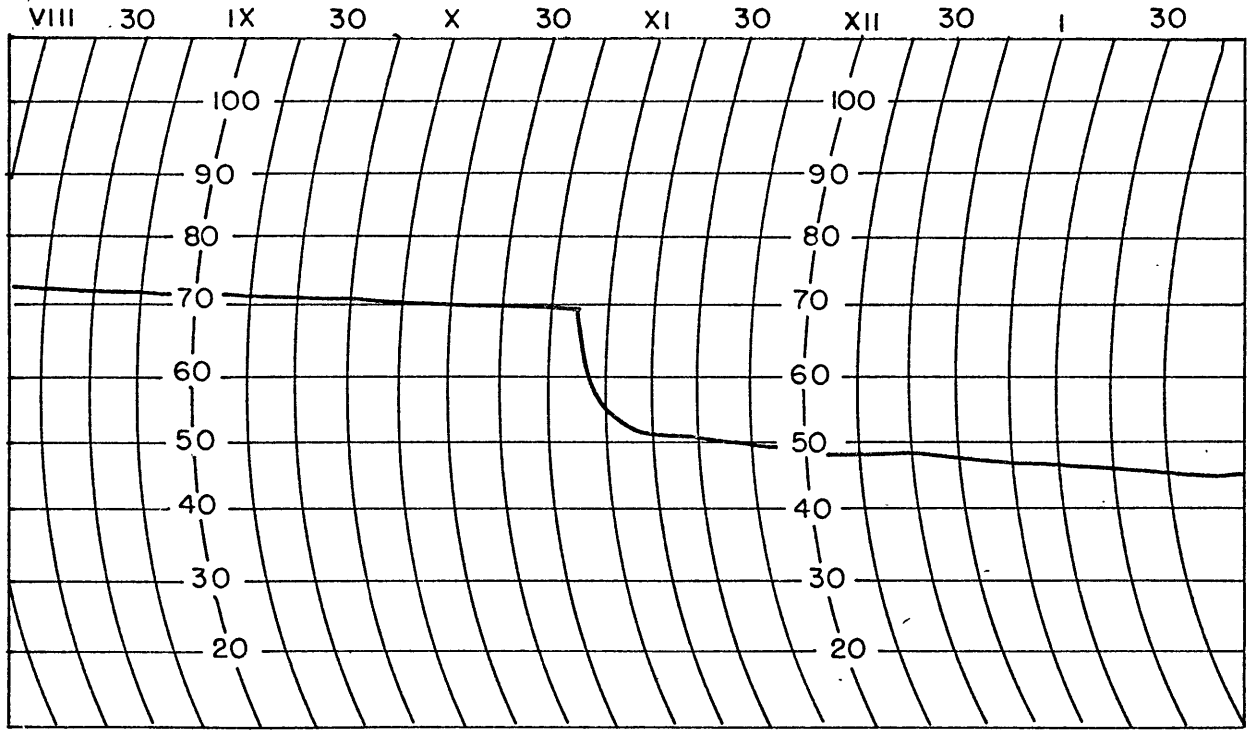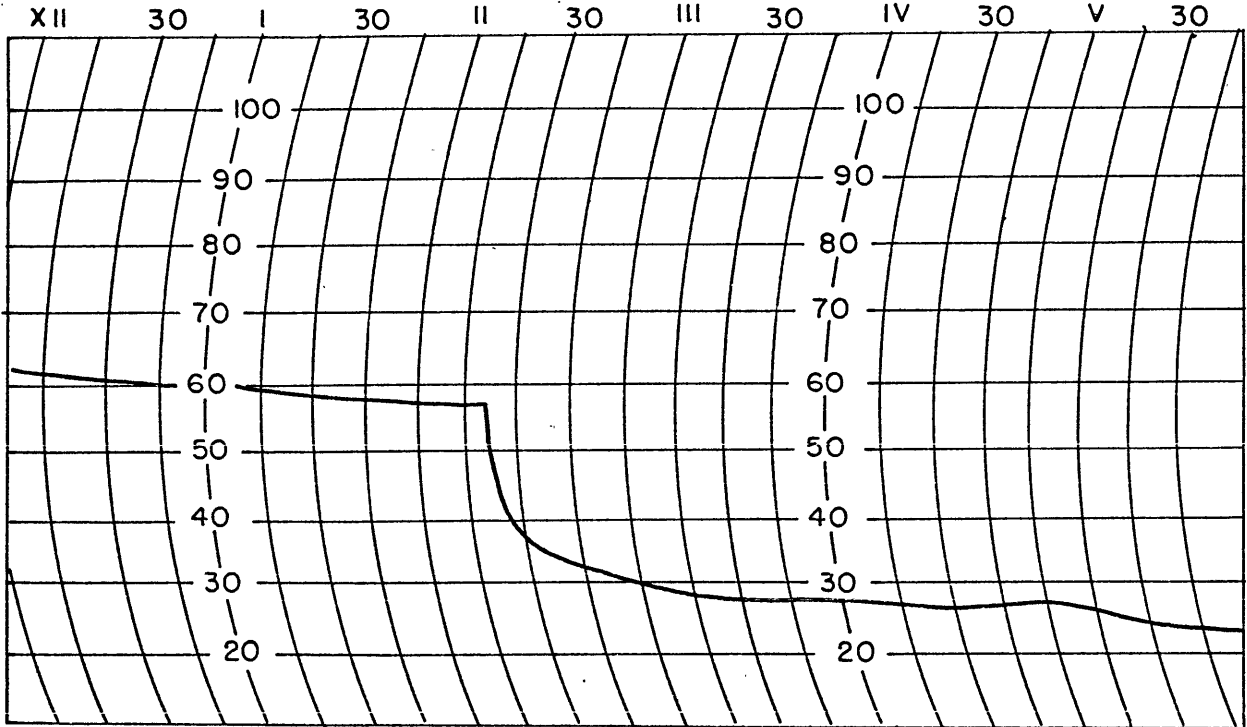T

P-2

P-1

.P
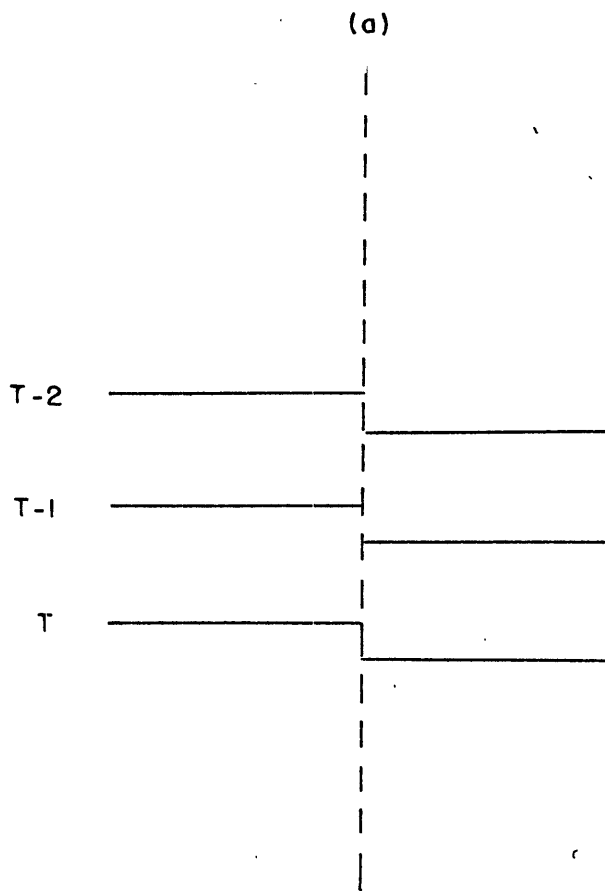
ZERO ORDER DISCONTINUITY
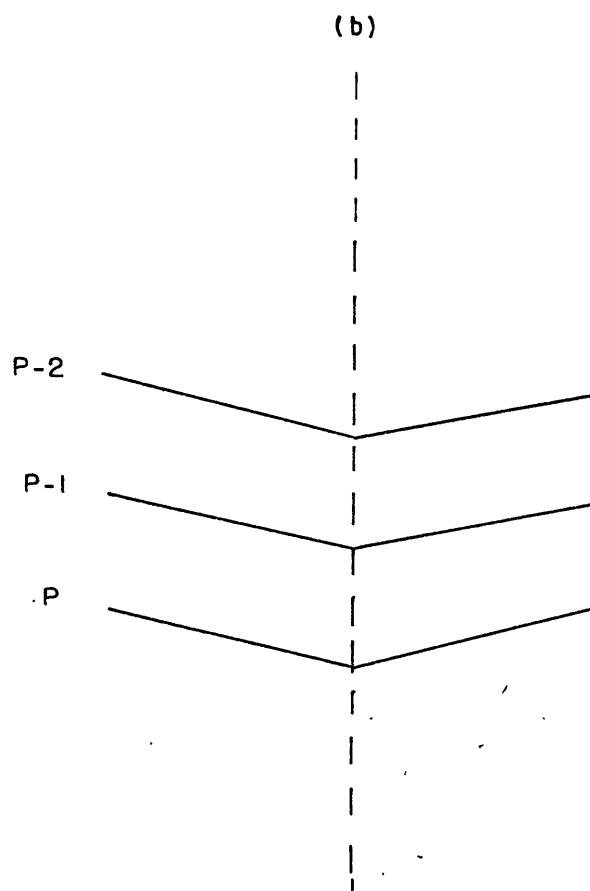
FIRST ORDER DISCONTINUITY

FIG. 1

COUGAR , OKLA.   MARCH 24, 1964

EL RENO , OKLA.   MARCH 23, 1965

FIG. 2

discontinuities in the temperature field, which can be shown to
be convenient mathematically.

For hydrodynamic reasons, this idealized front must satisfy
a dynamic boundary condition. This condition requires that
pressure be continuous across an internal boundary. If a zero
order discontinuity in pressure existed, we would be dealing
with a finite change in pressure through an infinitely small
distance and therefore with an infinite pressure gradient force.
Since this is impossible, a front may have a theoretical zero
order discontinuity with respect to temperature, but must have
of first order with respect to pressure. If geostrophic flow
is assumed, the dynamic boundary condition can be shown to
require a wind-shift across the frontal surface.

Much confusion now exists in the field of Meteorology
concerning fronts, their dynamics, and representation on daily
weather maps. There are even those who deny the existence of
fronts altogether, and it is to these skeptics that we address
figure 2. The Weather Bureau has not helped this confusion. It
has been suggested that fronts be omitted from their facsimile
products so that local forecasters might analyze them indepen-
dently. In the absence of precipitation, the two most important
characteristics of a frontal passage are the temperature break
and the wind-shift. The dynamic boundary condition requires a
wind-shift to accompany the temperature break. Frequently
these two events do not occur simultaneously, and therefore

some confusion exists regarding which event represents the

true front. In this study a front will be understood as

representing the previously mentioned "zone of rapid tempera-

ture transition." This choice is not made arbitrarily. It

is made because we feel that the temperature break is the more

significant of the two events. The timing between the wind-

shift and the temperature break and its relation to fronto-

genesis and frontolysis will be examined in a later section.

Now that we have defined a front, we will examine the important

process of frontogenesis.

Frontogenesis- Bergeron (1928) introduced the term "fronto-

genesis" as the tendency to create new fronts or intensify

existing ones, and "frontolysis" as the tendency to destroy

such zones. The frontogenetical function was first introduced

by Petterssen (1936)

$$F = \frac{d}{dt}\left|\nabla T\right| , \quad \nabla T = \frac{\partial T}{\partial x}\underline{i} + \frac{\partial T}{\partial y}\underline{j} + \frac{\partial T}{\partial z}\underline{k} \quad (1)$$

where the operator $\frac{d}{dt}$ is a process following a specific air

parcel, and represents temperature a scalar quantity. A

value of $F > 0$ gives frontogenesis, $F < 0$ frontolysis.

$$F = \frac{d}{dt}\left|\nabla T\right| = \frac{1}{2\left|\nabla T\right|} \frac{d(\nabla T \cdot \nabla T)}{dt} = \underline{N_T} \cdot \frac{d(\nabla T)}{dt} \quad (2)$$

where $\underline{N_T}$ is unit vector in direction of $\nabla T'$. Now expanding

$$\frac{d}{dt}(\nabla T') = \frac{\partial(\nabla T')}{\partial t} + u\frac{\partial(\nabla T')}{\partial x} + v\frac{\partial(\nabla T')}{\partial y} + \omega\frac{\partial(\nabla T')}{\partial z}$$

$$= \nabla\left(\frac{\partial T'}{\partial t}\right) + \nabla\left(\frac{u\partial T'}{\partial x}\right) + \nabla\left(v\frac{\partial T'}{\partial y}\right) + \nabla\left(\omega\frac{\partial T'}{\partial z}\right)$$

$$- \frac{\partial T'}{\partial x}\nabla u - \frac{\partial T'}{\partial y}\nabla v - \frac{\partial T'}{\partial z}\nabla\omega$$

$$= \nabla\left(\frac{dT'}{dt}\right) - \left(\frac{\partial T'}{\partial x}\nabla u + \frac{\partial T'}{\partial y}\nabla v + \frac{\partial T'}{\partial z}\nabla\omega\right) \quad (3)$$

it follows from equation (2) and (3)

$$F = \underline{N_T}\cdot\nabla\left(\frac{dT'}{dt}\right) - \underline{N_T}\cdot\left(\frac{\partial T'}{\partial x}\nabla u + \frac{\partial T'}{\partial y}\nabla v + \frac{\partial T'}{\partial z}\nabla\omega\right) \quad (4)$$

$$= \underline{N_T}\cdot\nabla\left(\frac{dT'}{dt}\right) - |\nabla T'|\frac{\partial V_n}{\partial n} \quad (5)$$

The first term on the right represents frontogenesis through diabatic processes. In the second term $|\nabla T'|$ is the magnitude of the temperature gradient, V is the velocity, and n is in the direction normal to the isotherms and towards the cold air. Thus if diabatic processes are absent and the wind has a component normal to the isotherms which decreases in its downstream direction figure 3, frontogenesis is to be expected; if the reverse occurs we have frontolysis.

Bergeron (1928) investigated the behavior of isotherms in a linear field of temperature, superimposed on a linear field of
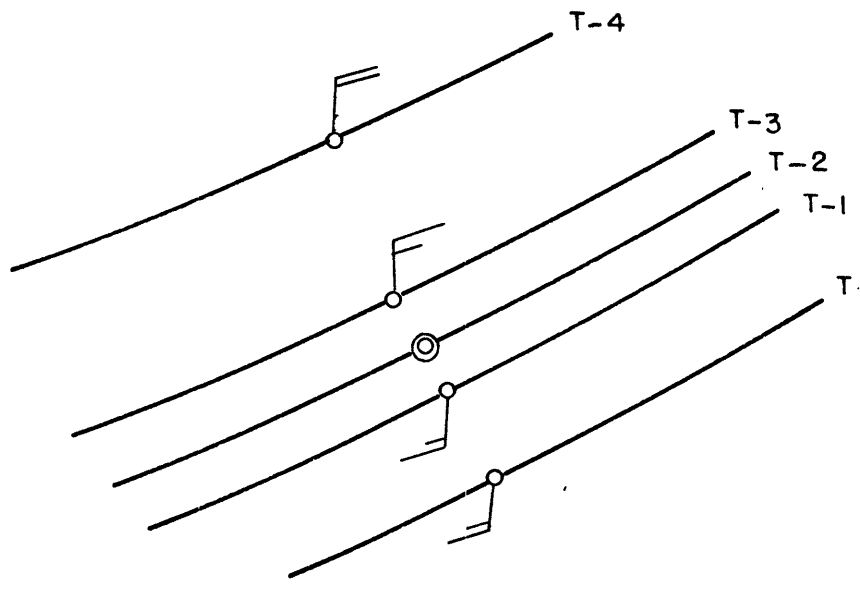
FRONTOGENESIS
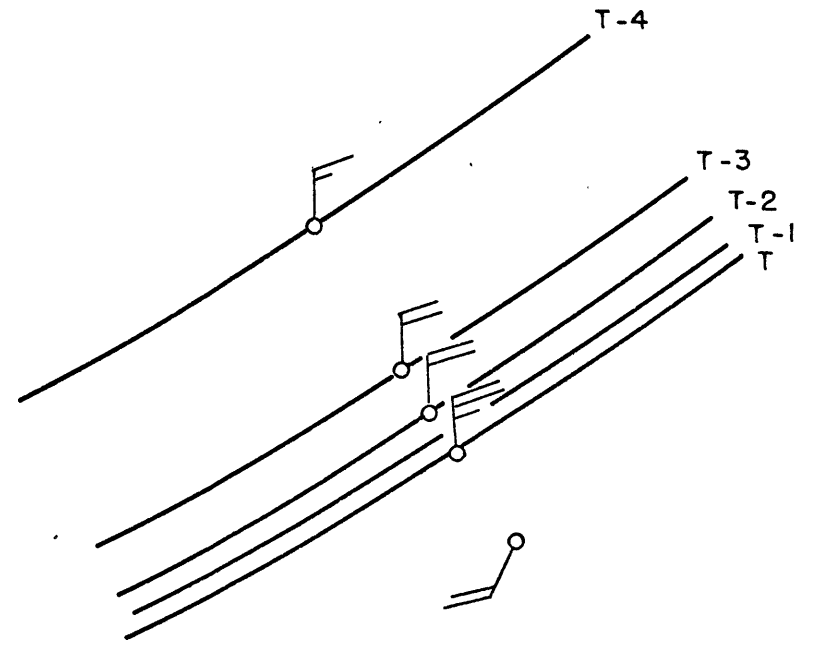
FRONTOGENESIS

FIG. 3

motion. He assumed that the velocity in the vicinity of a

point may be represented by its Taylor Series approximation

$$u = U_c + \left(\frac{\partial u}{\partial x}\right)_0 x + \left(\frac{\partial u}{\partial y}\right)_0 y + \frac{1}{2}\left(\frac{\partial^2 u}{\partial x^2}\right)_0 x^2 + \frac{1}{2}\left(\frac{\partial^2 u}{\partial y^2}\right)_0 y^2 + \left(\frac{\partial^2 u}{\partial x \partial y}\right)_0 xy + \cdots$$

$$v = V_0 + \left(\frac{\partial v}{\partial x}\right)_0 x + \left(\frac{\partial v}{\partial y}\right)_0 y + \frac{1}{2}\left(\frac{\partial^2 v}{\partial x^2}\right)_0 x^2 + \frac{1}{2}\left(\frac{\partial^2 v}{\partial y^2}\right) y^2 + \left(\frac{\partial^2 v}{\partial x \partial y}\right) xy + \cdots$$

In a sufficiently small area around the point in question, the

higher order terms in x and y may be neglected. We may write

this linear field

$$u \approx U_0 - \frac{1}{2}\left(\frac{\partial v}{\partial x} - \frac{\partial u}{\partial y}\right)_0 y + \frac{1}{2}\left(\frac{\partial u}{\partial x} + \frac{\partial v}{\partial y}\right)_0 x$$
$$+ \frac{1}{2}\left(\frac{\partial u}{\partial x} - \frac{\partial v}{\partial y}\right)_0 x + \frac{1}{2}\left(\frac{\partial v}{\partial x} + \frac{\partial u}{\partial y}\right)_0 y$$

$$v \approx V_0 + \frac{1}{2}\left(\frac{\partial v}{\partial x} - \frac{\partial u}{\partial y}\right)_0 x + \frac{1}{2}\left(\frac{\partial u}{\partial x} + \frac{\partial v}{\partial y}\right)_0 y$$
$$- \frac{1}{2}\left(\frac{\partial u}{\partial x} - \frac{\partial v}{\partial y}\right)_0 y + \frac{1}{2}\left(\frac{\partial v}{\partial x} + \frac{\partial u}{\partial y}\right)_0 x \tag{6}$$

where the velocity components are a combination of translation,

rotation, divergence, stretching deformation and shearing

deformation terms respectively. With the proper rotation of

principal axes, it may be shown that the last terms are zero

so that the velocity field can be written

$$u = (a+b)x - cy$$
$$v = cx + (b-a)y \tag{7}$$

where U_c and V_0 vanish with a parallel transition, and where

$$a = \frac{1}{2}\left(\frac{\partial u}{\partial x} - \frac{\partial v}{\partial y}\right) \text{ deformation,} \quad b = \frac{1}{2}\left(\frac{\partial u}{\partial x} + \frac{\partial v}{\partial y}\right)$$

divergence, and $c = \frac{1}{2}\left(\frac{\partial v}{\partial x} - \frac{\partial u}{\partial y}\right)$ vorticity. If we choose the

angle β between the x' axis and the isotherms figure 4, and

consider only the horizontal wind field then from equation (4)

$$F = D - \underline{N_T} \cdot \left(\frac{\partial T}{\partial x'} \nabla u + \frac{\partial T}{\partial y'} \nabla v \right)$$

where

$$D = \underline{N_T} \cdot \nabla \left(\frac{dT}{dt} \right)$$

and where the arbitrary coordinates x', y' are respectively

along and perpendicular to the axis of dilatation. Using fact

that

$$\frac{\partial T}{\partial x'} = |\nabla T| \cos \beta \qquad \frac{\partial T}{\partial y'} = -|\nabla T| \sin \beta$$

and equations 7 and 4

$$F = D - \left(\cos \beta \underline{i} + \sin \beta \underline{j} \right) \cdot |\nabla T| \left\{ \cos \beta [(a+b)\underline{i} \right.$$

$$\left. - c\underline{j} \right] + \sin \beta \left[c\underline{i} + (b-a)\underline{j} \right] \right\}$$

$$= D + \nabla T \left[(a+b) \cos^2 \beta - (b-a) \sin^2 \beta \right]$$

$$= D + |\nabla T| \left(a \cos 2\beta - b \right) \qquad (8)$$

The argument leading to the derivation of this equation

appears to be based on the assumption of a linear velocity

field. It is common practice among Meteorologists to begin

a derivation of equation 8 with this assumption. However,

equation (6) is simply an identity utilizing the derivatives

of u and v with respect to x and y and reduces to the statements
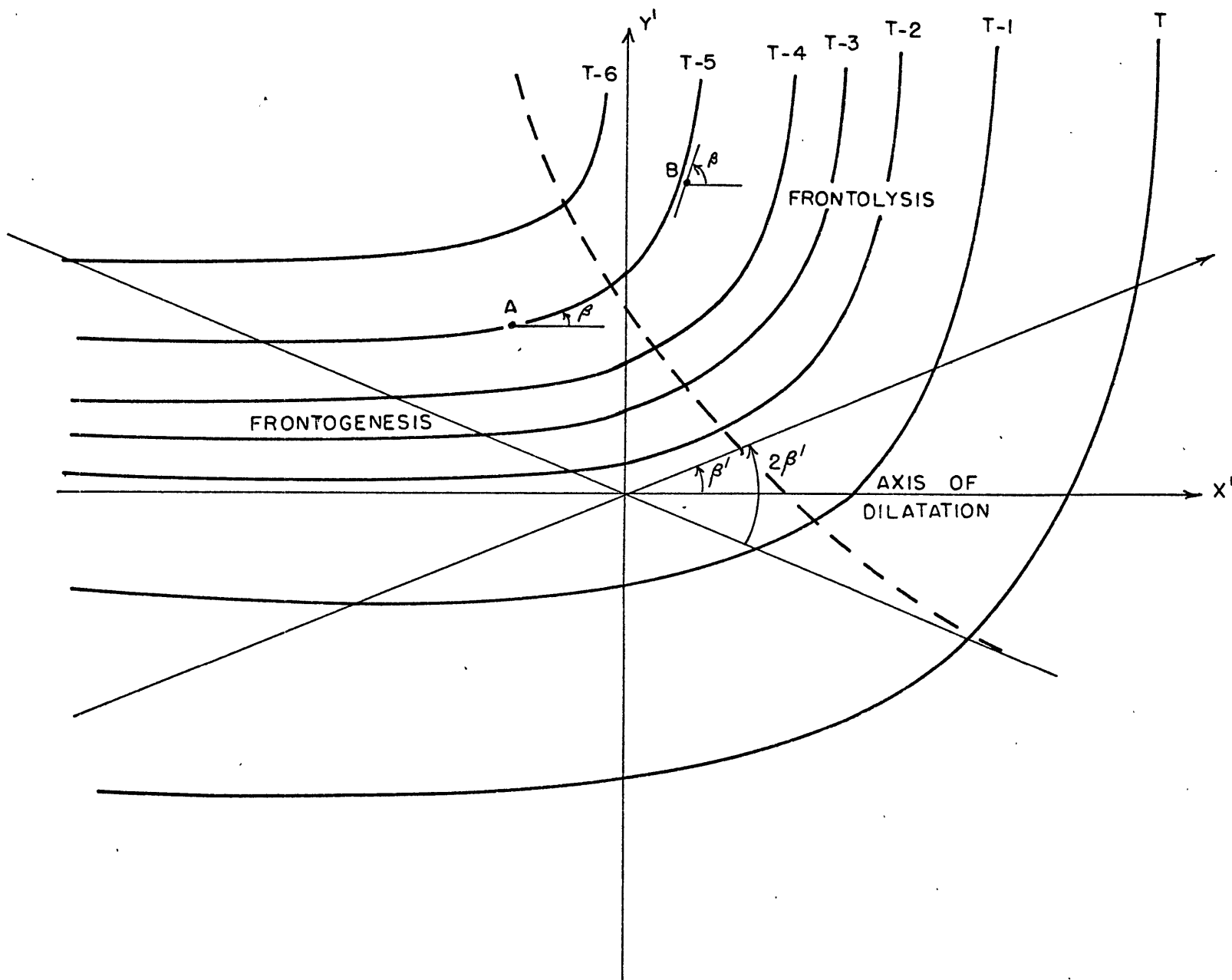
FIG. 4

$$\mu \approx \mu_0 \qquad\qquad v \approx v_0$$

The fact that the velocity fields are actually non-linear

does not invalidate the use of equation (6) except when

the distances x and y are very large. We will assume

linear velocity fields in this paper because finite differ-

ence methods are used and require the velocity to remain

linear over a grid interval. Equation (6) will simply be

used as a definition of divergence, vorticity and deforma-

tion. Therefore, although we will assume a linear velocity

field, it is not a necessary condition for the validity of

equation (8).

If we assume for the moment that the temperature is

a conservative property, then $D = 0$ and the

sign of F in equation (8) is determined by the angle β

for any given field of motion. Only deformation and

divergence can contribute to frontogenesis $F > 0$

and frontolysis $F < 0$. Furthermore, in

equation(8)convergence ($b < 0$) promotes fronotgenesis; and

divergence ($b > 0$), frontolysis. The angle for which

$F = 0$ in equation(8) is

$$\beta' = \frac{1}{2} \cos^{-1} \frac{b}{a}$$

If the divergence ($b = 0$), then $\beta' = \pm 45°$. When

there is convergence ($b < 0$), $\beta' > \pm 45°$; when

there is divergence ($b > 0$), $\beta' < \pm 45°$. In figure

4, we note that $\beta' < \pm 45°$ and so divergence has narrowed

the frontogenetical sector between $\pm \beta'$. At point A the

angle β , between the tangent to the isotherm and the

axis of dilatation, is less than angle β' , at point B it is

greater. Thus we have fronotgenesis at point A, frontolysis

at point B, and the dashed line separates the two areas for

this particular isotherm orientation.

Purpose- The purpose of this paper is to investigate the meso-

scale processes involved in frontogenesis. To gain insight

into these processes first it was necessary to determine

what characteristics of fronts are germane to our investigation.

Secondly, we use deformation fields in our analysis of fronto-

genesis in the hope that they will help us understand these

highly complicated processes. No similar work on this scale

has been done, although Williams(1962)investigated microscale

deformation and frontogenesis patterns near squall lines. If

we compare equations (5) and (8),

$$F = D - |\nabla T| \frac{\partial V_n}{\partial n} \quad , \quad F = D + |\nabla T| \left(a \cos 2\beta - b \right)$$

it appears that we have substituted a more complex expression
of the velocity field for a simpler one. Historically the
justification for this was that the Norwegian School originally
pictured air-masses ascending and descending relative to each
other at the frontal surface. This picture of frontogenesis
implies convergence associated with these motions. Later,
Bergeron (1928) showed that frontogenesis could be caused by
deformation in the absence of convergence. In this paper,
equation (8) is chosen to determine how important mesoscale
deformation is to frontogenesis.

In the final section, the relation between the wind-
shift and the temperature break accompanying frontal passage
is investigated. We hope that it will shed some light on
earlier investigations of this phenomenon by Plotkin (1965)
and Sanders (1966).

Data- The opportunity to study the mesoscale structure of fronts
was afforded by the establishment of the Beta Network by the
National Severe Storms Laboratory. The network was created to
study severe weather phenomena, i.e., thunderstorms and tornadoes,
which often occur in the Southern Plains during the Spring.

In 1964 it consisted of 41 stations spaced at ten to fifteen
mile intervals, located roughly between the Texas border and
Oklahoma City. During 1965 eleven more stations were added
to the southwest and north of the network. All stations
record data continuously during the months March through June
in graphic form consisting of station pressure, temperature,
relative humidity, wind direction, wind speed, and rainfall.
Of these, only wind speed, wind direction, and temperature were
used. Wind speed and direction were measured from wind towers
20 feet above ground, wind direction being recorded at one-
minute intervals and to 16 points of the compass. Wind speed
is recorded continuously and can be read accurately to the
nearest knot. Temperature was recorded continuously on a
thermograph figure 2, accurate to nearest 0.5°F. Pressure
was not analyzed because the barographs do not give station
pressures accurately during the periods of interest. We will
examine three cold front passages through the Beta network
during the 1964 and 1965 seasons. These cases are March 24,
1964; March 23, 1965; and April 24, 1965. They vary in inten-
sity, but have the common property of being essentially dry
with little if any frontal precipitation. These results are
at variance with those of Eliassen(1959)who professes that no
fronts exist without associated precipitation.

Computations- The time when each of these fronts most nearly
bisected the network was chosen for particular attention, and
the winds and temperatures were plotted from the continuously
recorded data. We made the rather crude assumption that each
front had a characteristic orientation at this time. This
orientation was chosen by drawing a straight line which most
closely approximated the leading edge of the cold air. We
decomposed the wind fields into u and v components relative to
this orientation. Using finite difference methods, the quanti-
ties $\frac{\delta v}{\delta x}$, $\frac{\delta v}{\delta y}$, $\frac{\delta u}{\delta x}$, and $\frac{\delta u}{\delta y}$ were evaluated midway between
grid points whose interval was nine nautical miles. The various
combinations of these quantities yield those components of
the velocity field discussed earlier.

The isotherm field was constructed from the plotted values
of temperature in whole degrees Fahrenheit. The values of
were determined by using finite differences over the same grid
interval. We neglect the differences in station elevation and
gradients of pressure, but the maximum possible error is 1°F
per nine nautical miles. Since the temperatures are read only
to the nearest degree, and since the actual gradients are as large
as 19°F per nine nautical miles, this approximation is considered
sufficiently good for the cases studied.

Using an average frontal orientation the angle β was
computed in the following manner following Saucier 1953. If
the u and v components of velocity and derivatives in the initial

(x,y) coordinate system are related to the velocity components u_1 and v_1 and derivatives in the $(x_1\ y_1)$ coordinate system, rotated counter-clockwise through the arbitrary angle

$$\mu = u_1 \cos\theta - v_1 \sin\theta \ ; \quad \frac{\partial}{\partial x} = (\cos\theta)\frac{\partial}{\partial x_1} - (\sin\theta)\frac{\partial}{\partial y_1}$$

$$v = u_1 \sin\theta + v_1 \cos\theta \ ; \quad \frac{\partial}{\partial y} = (\sin\theta)\frac{\partial}{\partial x_1} + (\cos\theta)\frac{\partial}{\partial y_1}$$

Then

$$\frac{\partial u}{\partial x} = \left[\left(\frac{\partial u_1}{\partial x_1}\right)\cos\theta - \left(\frac{\partial v_1}{\partial x_1}\right)\sin\theta\right]\cos\theta - \left[\left(\frac{\partial u_1}{\partial y_1}\right)\cos\theta - \left(\frac{\partial v_1}{\partial y_1}\right)\sin\theta\right]\sin\theta$$

$$\frac{\partial v}{\partial y} = \left[\left(\frac{\partial u_1}{\partial x_1}\right)\sin\theta + \left(\frac{\partial v_1}{\partial x_1}\right)\cos\theta\right]\sin\theta + \left[\left(\frac{\partial u_1}{\partial y_1}\right)\sin\theta + \left(\frac{\partial v_1}{\partial y_1}\right)\cos\theta\right]\cos\theta$$

$$\frac{\partial v}{\partial x} = \left[\left(\frac{\partial u_1}{\partial x_1}\right)\sin\theta + \left(\frac{\partial v_1}{\partial x_1}\right)\cos\theta\right]\cos\theta - \left[\left(\frac{\partial u_1}{\partial y_1}\right)\sin\theta + \left(\frac{\partial v_1}{\partial y_1}\right)\cos\theta\right]\sin\theta$$

$$\frac{\partial u}{\partial y} = \left[\left(\frac{\partial u_1}{\partial x_1}\right)\cos\theta - \left(\frac{\partial v_1}{\partial x_1}\right)\sin\theta\right]\sin\theta + \left[\left(\frac{\partial u_1}{\partial y_1}\right)\cos\theta - \left(\frac{\partial v_1}{\partial y_1}\right)\sin\theta\right]\cos\theta$$

a) $$\frac{\partial u}{\partial x} - \frac{\partial v}{\partial y} = \left[\left(\frac{\partial u_1}{\partial x_1}\right) - \left(\frac{\partial v_1}{\partial y_1}\right)\right]\cos 2\theta - \left[\left(\frac{\partial v_1}{\partial x_1}\right) + \left(\frac{\partial u_1}{\partial y_1}\right)\right]\sin 2\theta$$

b) $$\frac{\partial v}{\partial x} + \frac{\partial u}{\partial y} = \left[\left(\frac{\partial v_1}{\partial x_1}\right) + \left(\frac{\partial u_1}{\partial y_1}\right)\right]\cos 2\theta + \left[\left(\frac{\partial u_1}{\partial x_1}\right) - \left(\frac{\partial v_1}{\partial y_1}\right)\right]\sin 2\theta$$

The two types of deformation are dependent upon the orientation of the coordinates, and with the proper orientation one of these deformations may be eliminated. Choosing to eliminate the shearing deformation

c) $\quad \dfrac{\partial u}{\partial x} - \dfrac{\partial v}{\partial y} = \left[\left(\dfrac{\partial u_1}{\partial x_1} \right) - \left(\dfrac{\partial v_1}{\partial y_1} \right) \right] \cos 2\Theta$

d) $\quad \dfrac{\partial v}{\partial x} + \dfrac{\partial u}{\partial y} = \left[\left(\dfrac{\partial u_1}{\partial x_1} \right) - \left(\dfrac{\partial v_1}{\partial y_1} \right) \right] \sin 2\Theta$

dividing $\quad \tan 2\Theta = \dfrac{\left(\dfrac{\partial v}{\partial x} + \dfrac{\partial u}{\partial y} \right)}{\left(\dfrac{\partial u}{\partial x} - \dfrac{\partial v}{\partial y} \right)}$ $\qquad (9)$

thus the angle of required rotation is obtained from the ratio of the deformations in the initial coordinate system.

Neither deformation gives individually the total deformation unless the other is zero. To compute fields of deformation, we must combine the two types to give a resultant deformation. This is achieved in equations c) and d) where rotation of the coordinate axes through such an angle that in the new system one type of deformation vanishes. Thus if the shearing deformation is eliminated

$$DEF_R = \left(\dfrac{\partial u}{\partial x} - \dfrac{\partial v}{\partial y} \right) \sec 2\Theta \qquad (10)$$

If this arbitrary angle Θ is assumed to be equal to the angle β, we can compute the axis of dilatation for each station using equation 9. The absolute rate of deformation may be found using the appropriate shearing deformation and angle , equation 10. Finally with the temperature gradient, divergence, deformation, and angle β, the kinematic term of frontogenetical function may be evaluated by equation (8) if we neglect the diabatic term D. This term and its contribution to the total rate of frontogenesis will be discussed in following sections.

In the final section, the structure of each of the three fronts is examined at all stations for the period surrounding the initial temperature break. The time of the break was estimated by use of thermograph traces, and was generally evidenced by an unmistakable break figure 2. The time of wind-shift was determined from the continuous wind records, and in all cases this shift was at least 22.5 degrees. The difference between these two times is calculated, and the wind field is examined in the immediate vicinity of the temperature break.
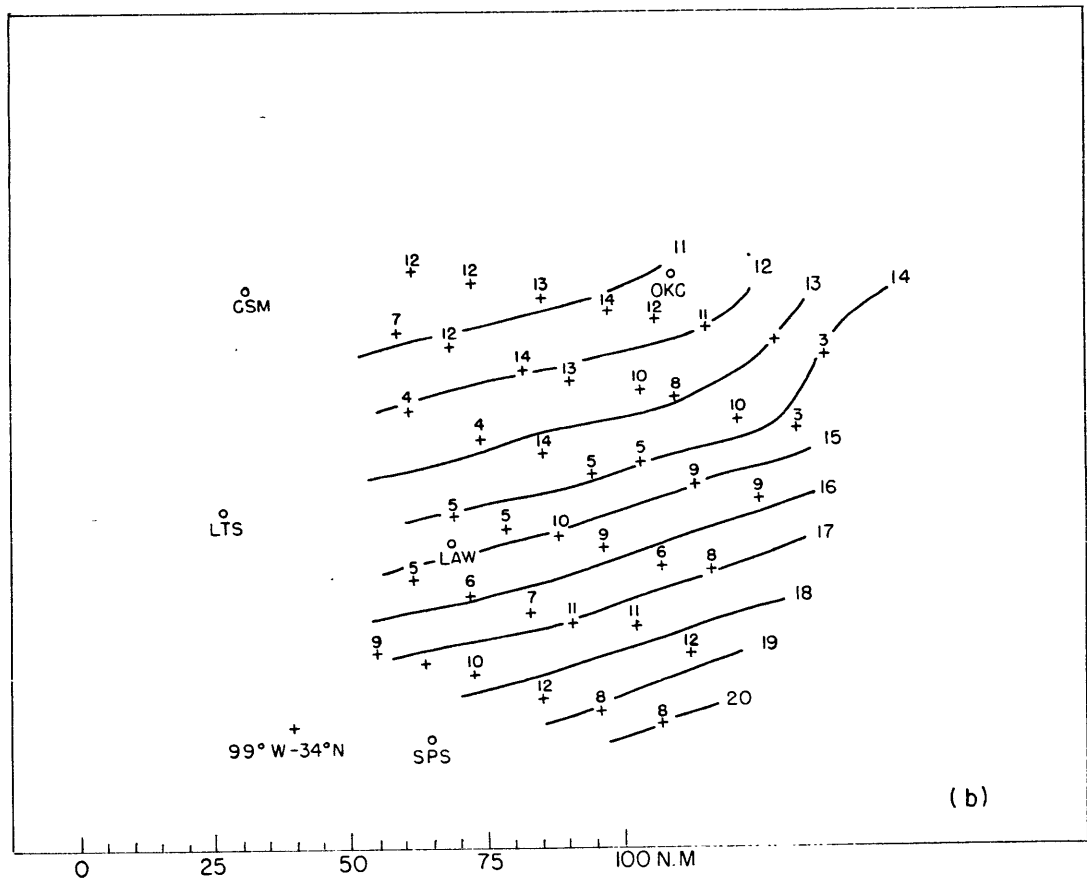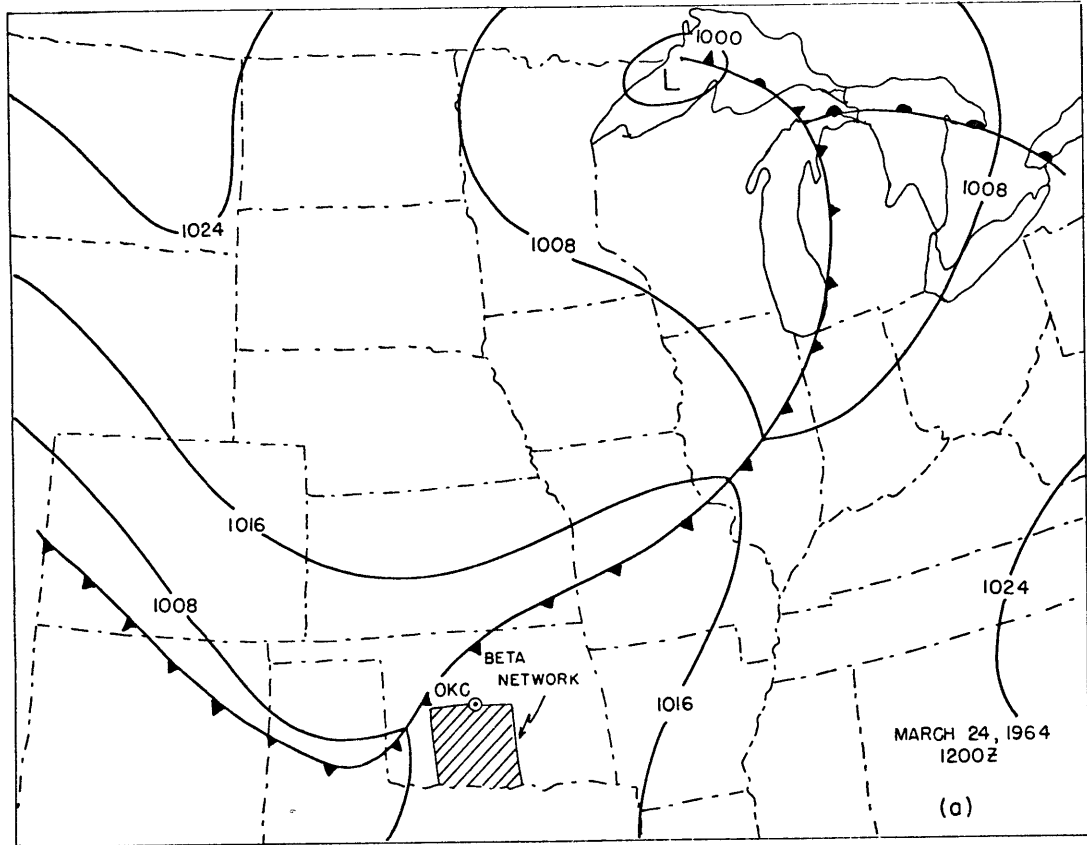
Results

Case I - March 24 1964

The surface chart for 1200 GMT figure 5a shows a cold front just northwest of the network with a closed low in the vicinity of Lake Superior. The front does not appear to be intense at this time, nor does it undergo any dramatic change while in the network. But upon leaving, a wave developed on the front which eventually became a major storm affecting the Northeast. The front was in the network between 1018 and 2023 CST and the hourly positions are indicated in figure 5b. It maintains an average speed of nine knots and has an average orientation of 250-070 degrees. It appears to move faster for the first four hours, but slows down after 1400 CST.

The nine-minute temperature drops at each station with usable data are shown above the station figure 5b with maximum drops of 14°F recorded at three stations, and an average drop for the network of 8.9°F. A small wave west of Oklahoma City increases amplitude with time, and appears to have developed into the major storm which affected the Northeastern States two days later. Although no significant precipitation accompanied the front, low ceilings associated with the develo-ping wave were reported on the hourlies at stations around the network. This prevented direct insolation before frontal pass-age. A few stations in the middle of the network reported scattered clouds prior to frontal passage. The destructive

March 24, 1964

figure 5 (a)   Surface Chart.

(b)   Hourly positions of front and nine-minute

temperature drops.

(a)

1000
L
1008
1024
1008
1016
1008
1016
1024
BETA NETWORK
OKC
MARCH 24, 1964
1200 Z

(b)

12
12
13
14
11
12
13
14
OKC
12
GSM
7
12
11
14
13
10
8
3
4
4
3
14
15
5
5
9
5
10
9
16
5
9
LTS
5
LAW
10
9
6
8
17
6
7
11
11
18
9
10
12
19
12
8
8
20
99° W-34°N
SPS

0   25   50   75   100 N.M

effect of insolation might explain some of the relatively small nine-minute temperature drops between 1300 CST and 1500 CST,

The wind field at 1400 CST figure 6a indicates the surface wind observations in knots, The divergence and vorticity fields at this time figures 6b and 6c are drawn for each 15 units of 10^{-4} sec^{-1}. Large values of convergence are found along the front with a maximum, in the vicinity of the small wave. The vorticity field has a maximum west of the maximum convergence zone, and has large values surrounding the wave with small values outside the frontal area.

The thermal field at 1400 CST figure 6d has a maximum temperature gradient in the eastern half of the front. A thermal ribbon exists within a grid interval behind the front and as we progress to the West, we note the destructive influence of the Wichita Mountains, north of Lawton. In the cold air to the north, there is a temperature differential greater than 30°F, while in the warm air to the south there is only 5°F differential.

The axes of dilatation, indicated by the double-ended arrows, are generally parallel to the front. At a distance greater than 15 miles from the front they become more normal.

The absolute magnitude of the resultant deformation figure 6e computed from equation 10 is drawn for each 15 units of 10^{-4} sec^{-1}. It also has a maximum in the vicinity of the

March 24, 1964

figure <u>6</u> (a) Surface wind observations in knots.

(b) Divergence in units x 10^{-4} sec^{-1}.

(c) Vorticity in units x 10^{-4} sec^{-1}.

(d) Isotherms in °F and axes of dilatation.

(e) Absolute magnitude of the resultant deformation in units x 10^{-4} sec^{-1}, computed from equation (10).

(f) Frontogenetical function in units °F/NM/HR, computed from non-diabatic terms in equation (8).

(a)

(b)

(c)

(d)

(e)

(f)
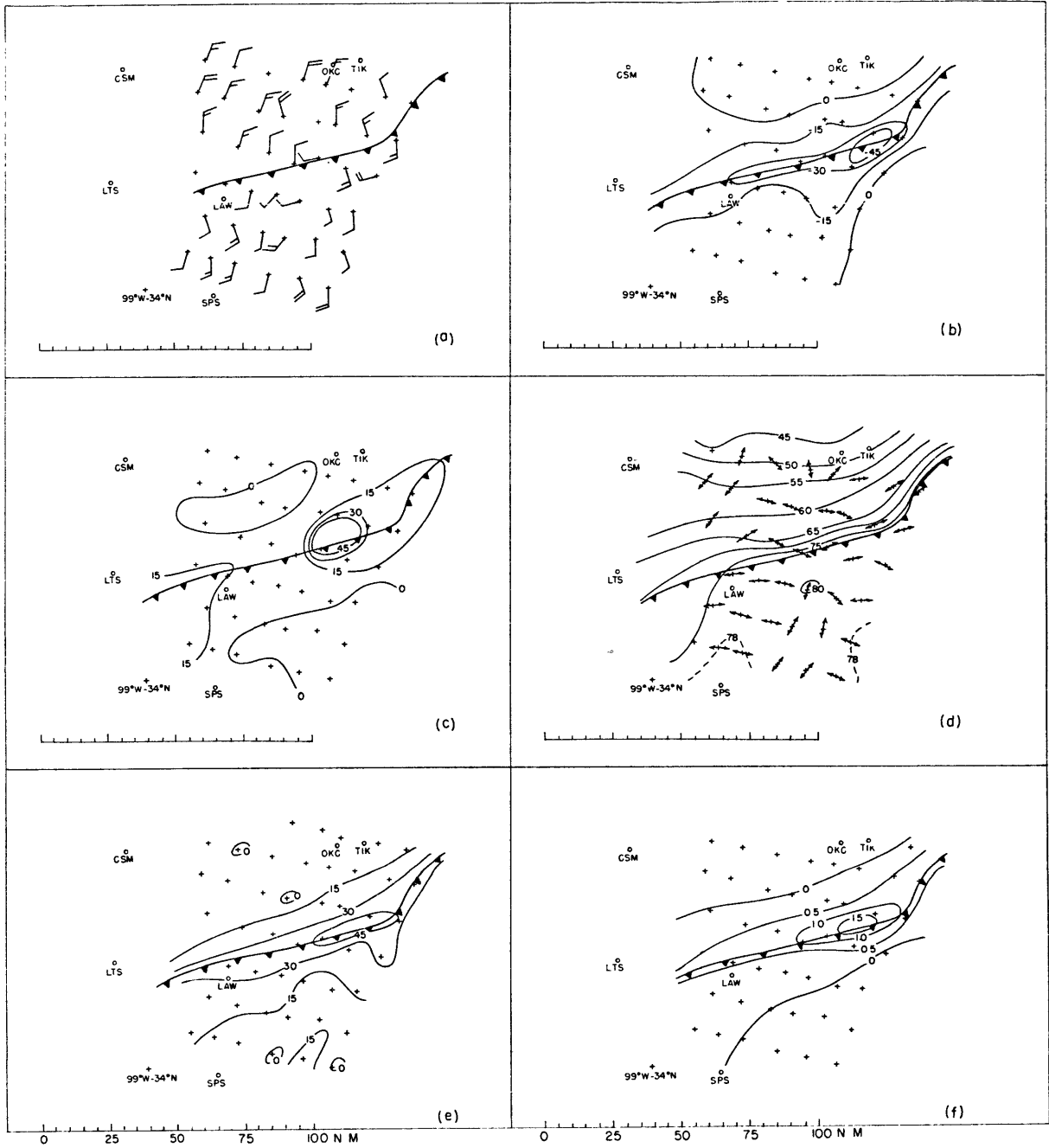
of the wave. Although it resembles the divergence pattern, the deformation is larger on the average and encompasses a broader area as we might expect.

The frontogenetical function figure 6f is given by equation (7) and naturally has its maximum where the favorable fields of convergence, deformation and temperature are coincident. Large values of frontogenesis measured in °F/nm/HR are found close to the leading edge of the front and extend well into the thermal ribbon behind the front. Frontolysis is noted well outside the frontal zone and should be expected to the South where there is negligible temperature gradient. To the north, there is a moderate temperature gradient but the axes of dilatation are mostly normal to the isotherms producing net frontolysis. It should be understood that this is an instantaneous picture of frontogenesis, and that although large values of frontogenesis will remain in the vicinity of the front, the maximum areas may migrate along the front.

Case II - March 23, 1965

During the 1965 season the Beta network added eleven new stations on the southwestern and northern boundaries of the network. At 0000 GMT figure 7a a rather diffuse stationary front is located north of Oklahoma. In the period of a few hours, it intensifies and comes through the network figure 7b with an average speed of 24 knots, producing nine-minute

March 23, 1965

figure 7 (a) Surface Chart.

(b) Hourly positions of front and nine-minute

temperature drops.

(a)

MARCH 23, 1965
0000 Ƶ

(b)

0   25   50   75   100 N.M.
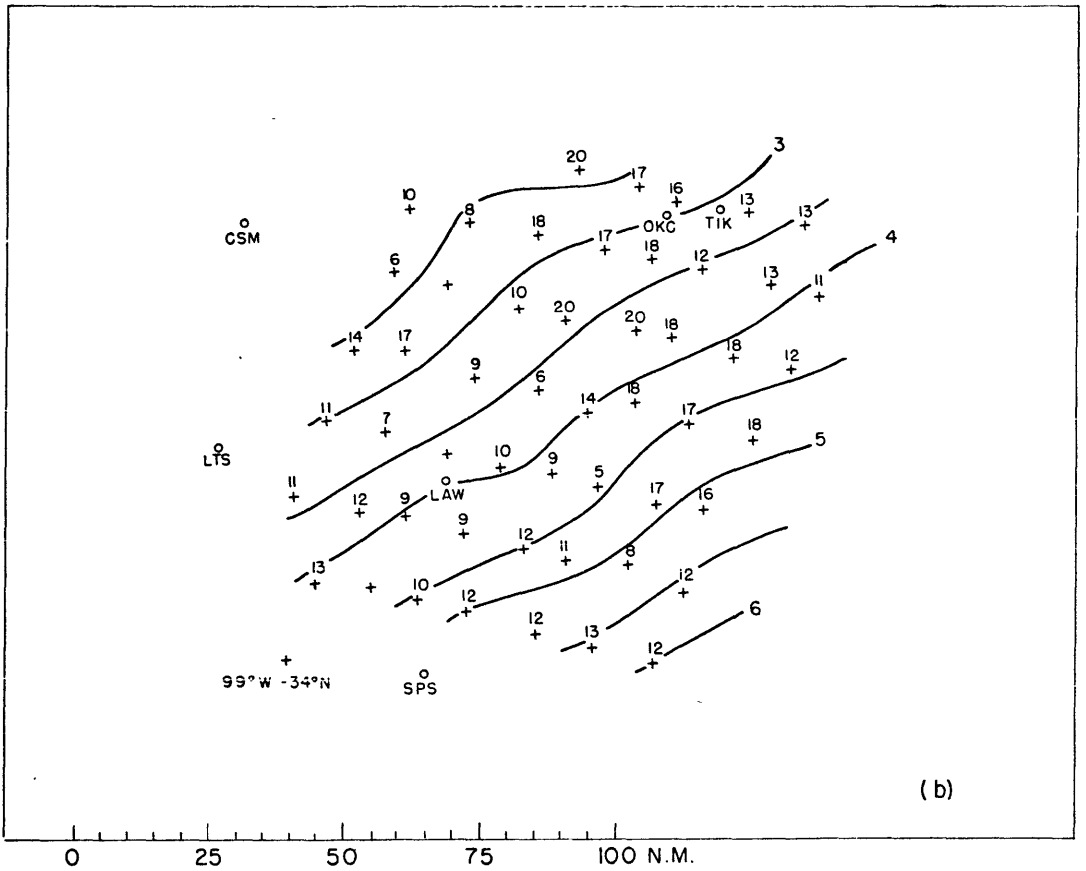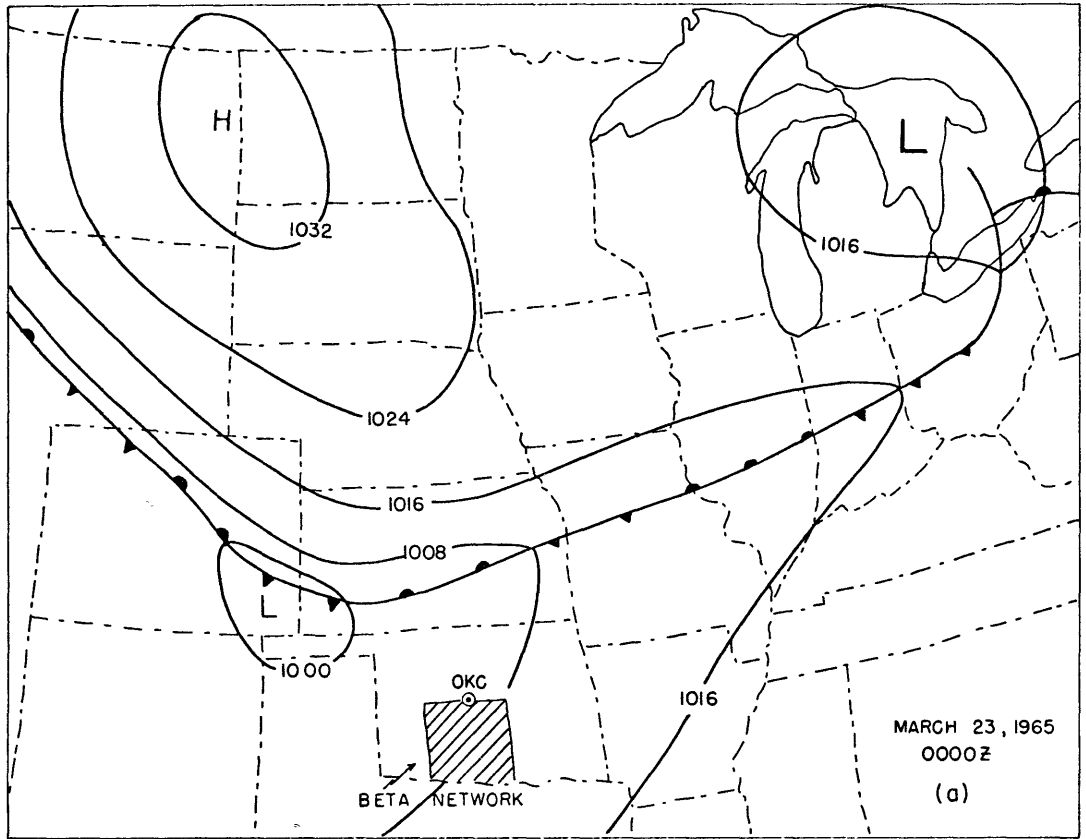
temperature drops of 20°F. The average drop for the 49 stations
with usable data over the nine-minute period, is 13.0°F, and
of the 49 stations, 43 demonstrates an unmistakable break similar
to figure 1. Two waves are present and the one to the northeast
appears to die as it leaves the network. The other, in the lee
of the Wichita Mountains, also appears to lose amplitude with
time. The front appears to be moving slightly faster as it
enters the network than when it leaves. It seems to undergo
some modification while within the network, at least with respect
to the nine-minute temperature drops. There is an unusual lack
of cloudiness in this case, and the typical reporting station
experiences at most only broken conditions. The early hour in
which this front came through the network would indicate that
the source of smaller nine-minute drops in the temperature to
the south, is other than insolation.

The wind field at 0400 CST figure 8a shows strong northerly
flow behind the front with weak southerly flow in advance. The
divergence pattern figure 8b has two large convergent areas
with the one to the southwest the more intense. Some small areas
of divergence are located behind the front which are evident from
the wind analysis figure 8a. The vorticity pattern figure 8c
has a large maximum behind the front to the northeast and a
secondary maximum to the southwest. An unusual value occurs in
the vicinity of the small wave east of the Wichita Mountains.
This maximum of anticyclonic vorticity occurs along the front

March 23, 1965

figure 8, notation same as in figure 6.

     (a)   Surface wind observations.

     (b)   Divergence.

     (c)   Vorticity.

     (d)   Isotherms and axes of dilatation.

     (e)   Absolute magnitude of the resultant deformation.

     (f)   Frontogenetical function.

(a)

(b)

(c)

(d)

(e)

(f)
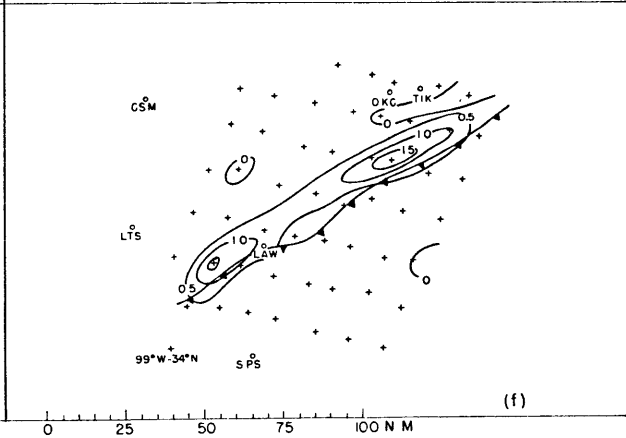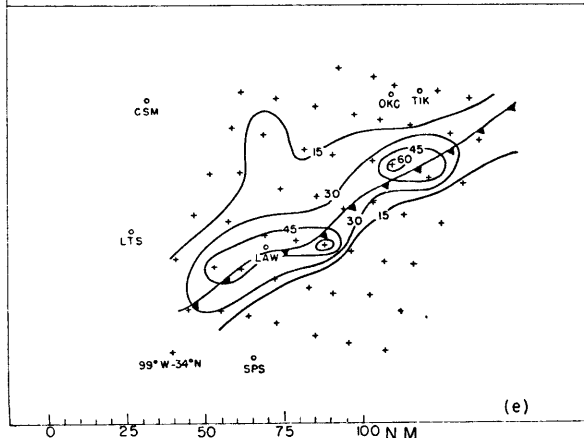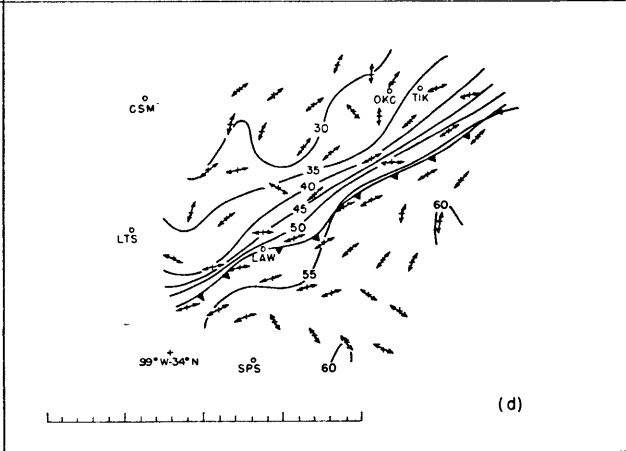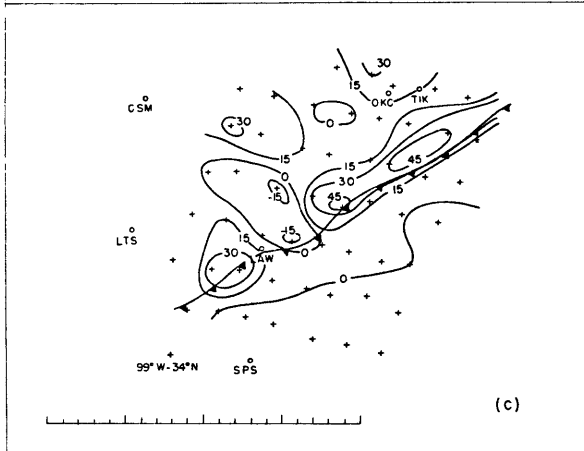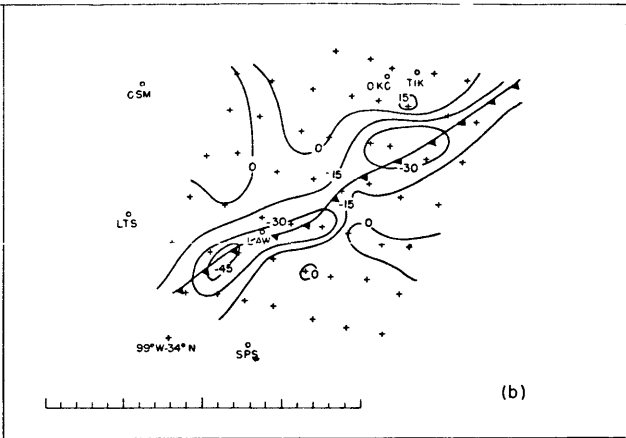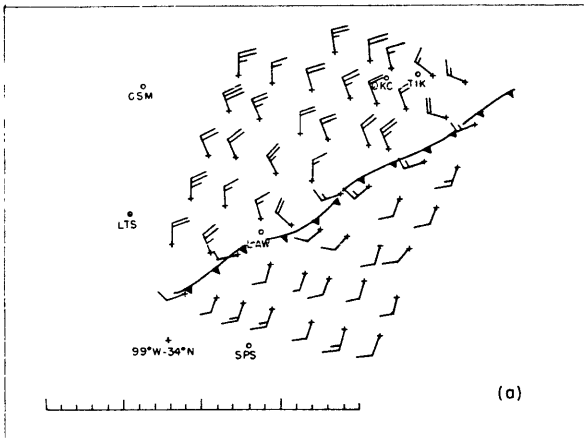
and it can be accounted for in the following manner. The oro-
graphic influence of the Wichita Mountains has a modifying

effect on the normal component of the wind, and thus as we

proceed eastward along the front in the positive x direction,

the normal component of wind increases and we get a large

negative $\frac{\partial v}{\partial x}$ (v being measured positive in the y direction.)

This large value of $-\frac{\partial v}{\partial x}$ dominates the term $\left(\frac{\partial v}{\partial x} - \frac{\partial u}{\partial y} \right)$,

and therefore anticyclonic vorticity is found along the front,

contrary to geostrophic expectations.

The temperature field figure 8d shows a very strong tempera-
ture gradient which extends 10 to 15 miles behind the front.

Again the effect of the Wichita Mountains is seen to the west

of Lawton. The temperature field in the warm air exhibits

little gradient while the contrast of temperatures in the cold

air is large. The axes of dilatation are mostly parallel to

the isotherms in the region of maximum temperature contrast

and remain parallel well into the warm air in advance of the

front. At distances greater than 25 miles, the axes become

more normal to the isotherms.

The deformation field figure 8e appears to be concentrated

slightly behind the front with large values of deformation

encompassing a major portion of the larger temperature gradients.

Again we note that the deformation field is broader and has

larger absolute values than the divergence field. The Wichita

Mountains are included in the southwestern maximum, which should

be expected as the wind must contract as it approaches the
mountains, producing deformation.

The frontogenetical function is concentrated in two areas
figure 8f. The effect of the divergence and lack of appreciable
temperature gradient is evident east of Lawton. The huge rates
of frontogenesis to the northeast and to the southwest corre-
spond well with the nine-minute temperature drops near and
downstream from these maxima figure 7b.

Case III - April 24, 1965

At 1200 GMT figure 9a, an unorganized stationary front is
located north of the network. It intensifies and twelve hours
later passes Oklahoma City as a weak cold front. Initially the
front is dry and therefore similar to the two previous cases.
However during the afternoon, thunderstorms developed in the
southern and southwestern portions of the network, and this
complicates the analysis of thermograph traces at a few stations.
The hourlies indicate scattered to broken sky conditions exist
before and after frontal passage at those stations north of the
2000 CST position. Maximum diurnal heating occurs in this area,
with temperatures reaching the mid eighties before passage.
South of the 2000 CST position figure 9b, thunderstorms reduce
the temperature at many stations and after sunset, sky conditions
were favorable for radiational cooling. The front was in the
network from 1649 CST to 0026 CST. It has an average speed of

April 24, 1965

figure 9 (a) Surface Chart.

    (b) Hourly positions of front and nine-minute
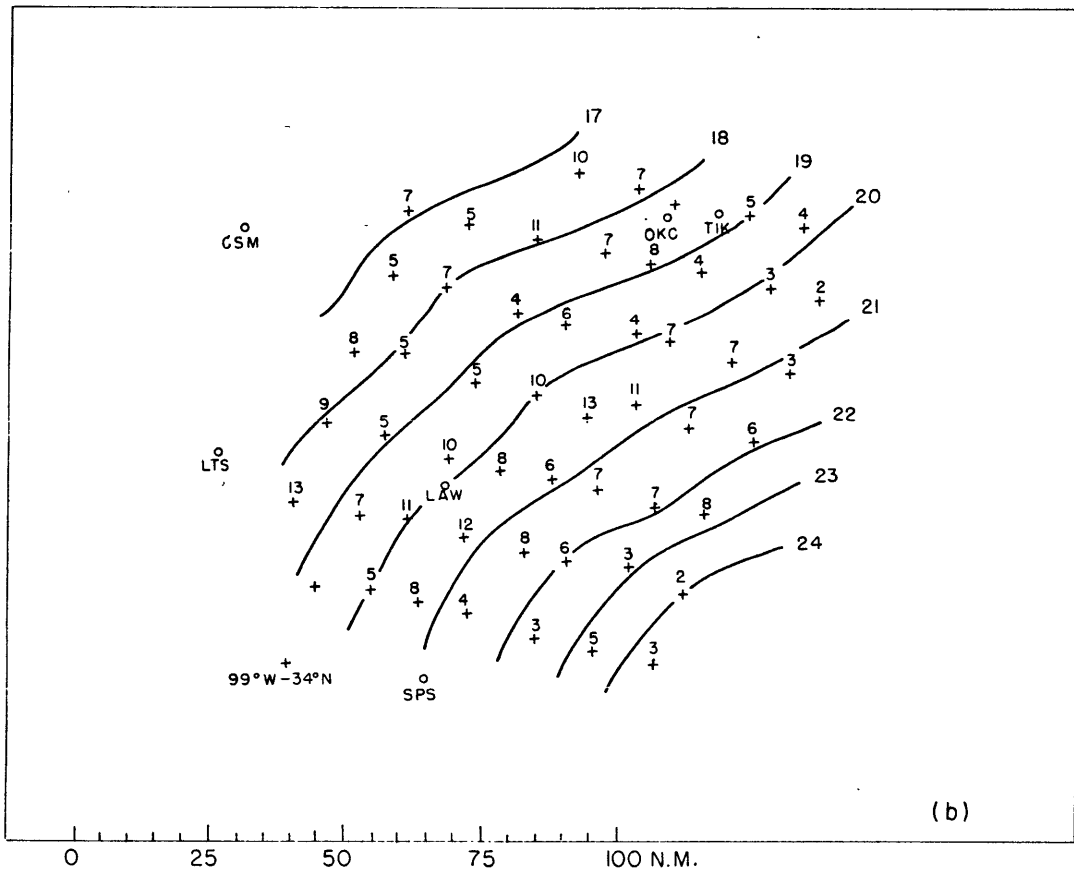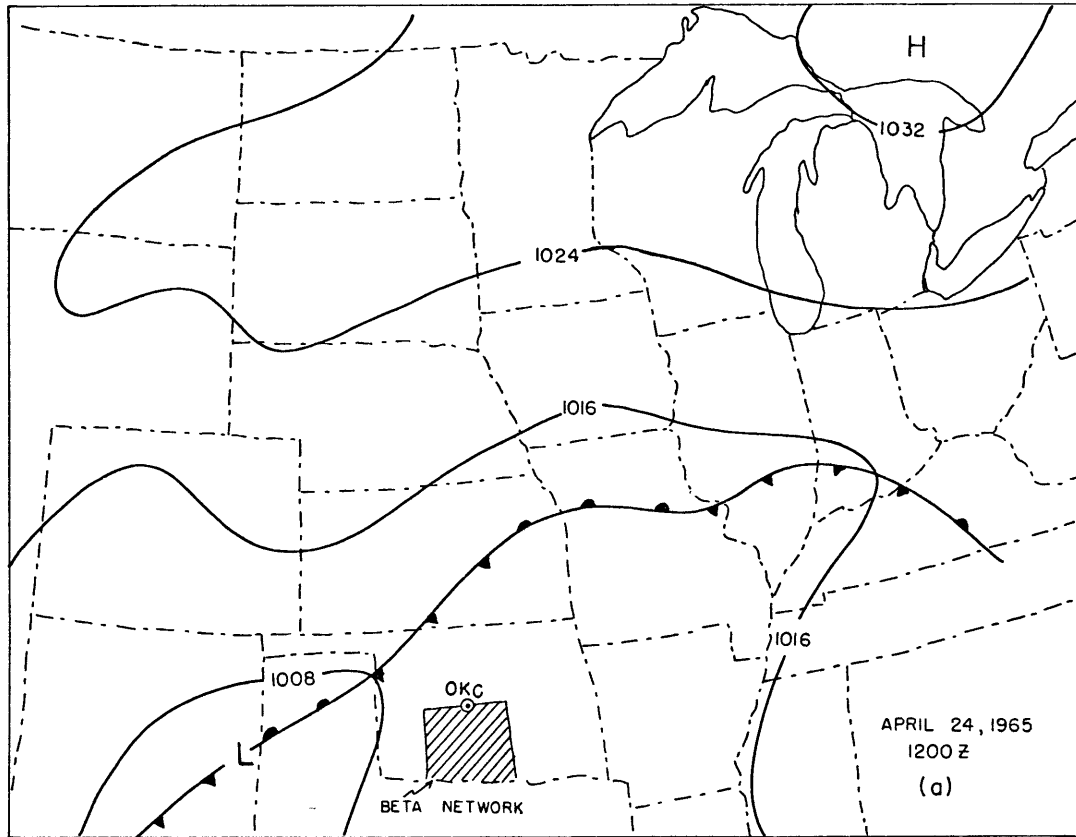
         temperature drops.

12 KTS, and an average frontal orientation of 230-050 degrees.
The maximum nine-minute temperature drops are 13°F with a
network average of 6.6°F for the 50 stations with readable
data. Rain associated with thunderstorms (↰) is reported at
almost all stations in the bottom two rows and naturally
modifies the temperature drop which would have otherwise
occurred. One small wave is present to the west and increases
amplitude near the Wichita Mountains, but loses its amplitude
soon after.

The wind field at 2000 CST figure 10a, indicates broad
convergence in the frontal zone. The divergence and vorticity
fields figures 10b and 10c, are generally symmetric with respect
to the front. Three large convergent areas lie along the front,
with a general broadening of the convergent region to the south-
west. A large divergent area to the south results from weak
southeasterly flow figure 10a at these stations with maximum
values of southeasterly flow closer to the front. The vorticity
pattern exhibits two maxima, one on either side of the small
wave. A large area of positive vorticity lies along the front,
and two small anticyclonic areas lie to the north.

The thermal gradient figure 10d is well organized in the
southwest and somewhat less well organized to the northeast.
The weak gradients to the northeast seem to be well correlated
with the small nine-minute temperature drops figure 9b.
The temperature field to the south is flat except for a moderate

April 24, 1965

figure 10, notation same as in figure 6.

      (a)   Surface wind observations.

      (b)   Divergence.

      (c)   Vorticity.

      (d)   Isotherms and axes of dilatation.

      (e)   Absolute magnitude of the resultant deformation.

      (f)   Frontogenetical function.

(a)

(b)

(c)

(d)

(e)

(f)
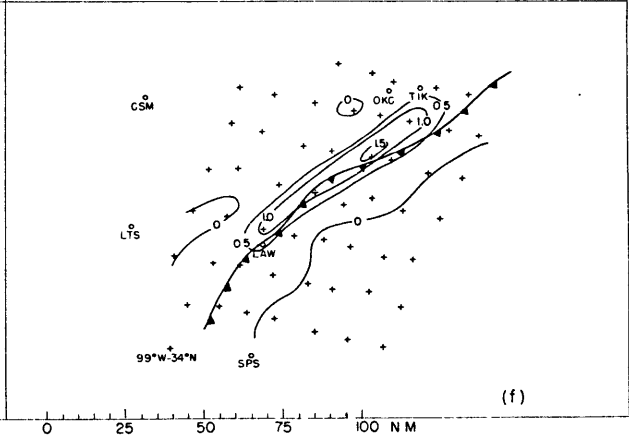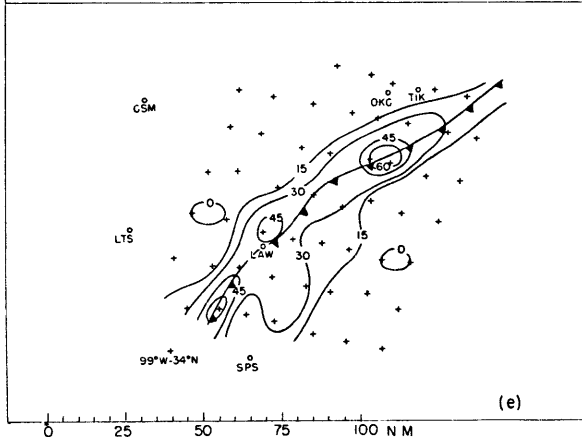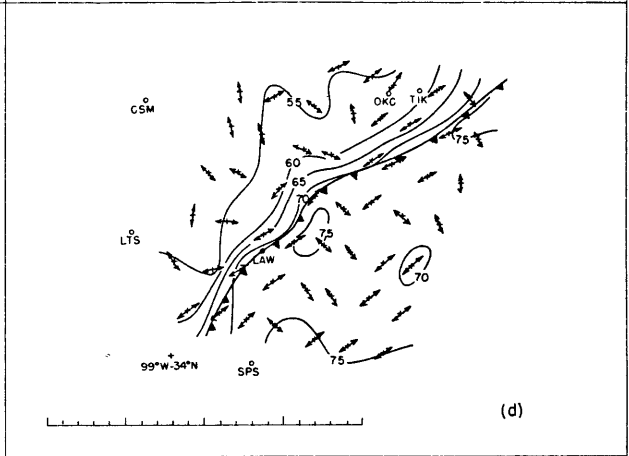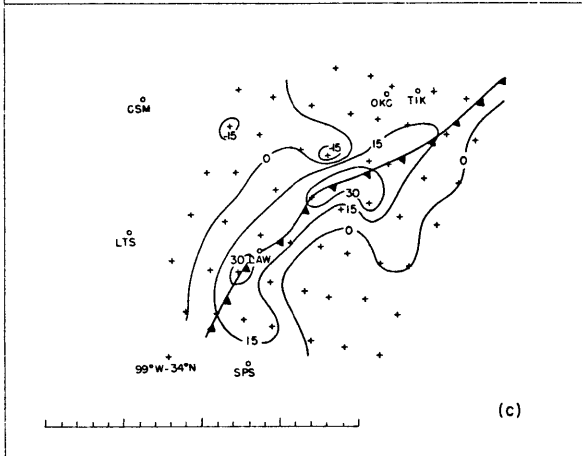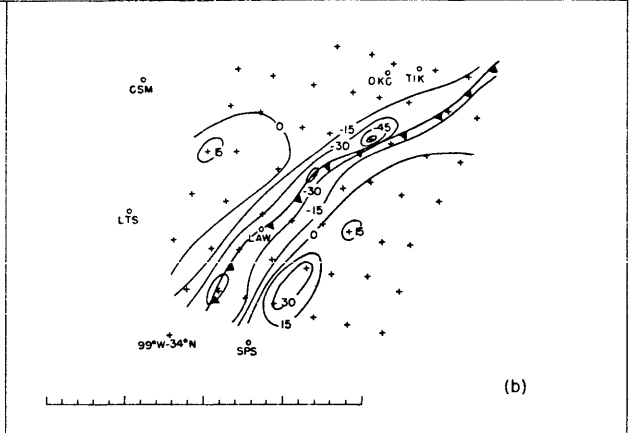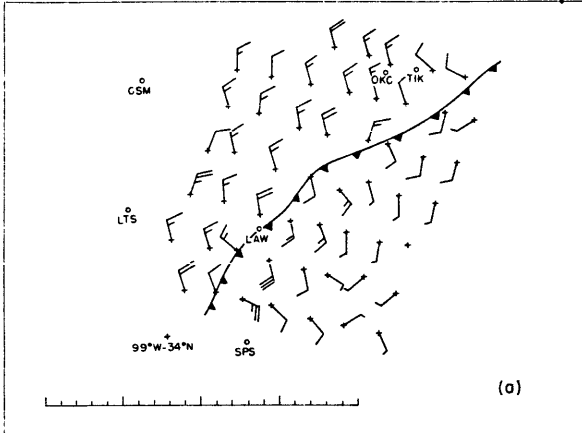
gradient ahead of the small wave. The dilatation axes are mostly parallel to the isotherms in the frontal zone with the notable exception of the northeastern sector. This is well correlated with the temperature drops. Outside a ten mile distance, the axes are poorly organized and tend to be normal to the isotherms.

The deformation field figure 10e is quite similar to the divergence pattern with two maxima along the front. The field is more intense and broader than the divergence field. Notice that the deformation field encompasses the area where large values of divergence were located in figure 10b.

The frontogenetical function figure 10f shows a huge rate of frontogenesis just behind the front where there is a favorable coincidence of convergence, deformation, and temperature gradient. This large area occurs in a region where the temperature gradient was relatively weak, but where the additive values of convergence and deformation produce huge rates of frontogenesis. With reference to the nine-minute temperature drops figure 9b, the front on the average appears to intensify the following hour, but then diabatic processes weaken it.

Conclusions

We have investigated the mesoscale kinematics of three cold fronts. These fronts were dissimilar first with respect to intensity if the nine-minute temperature breaks are to be used as criteria. Secondly the speeds differed considerably. One case required ten hours to traverse the network, while another required less than four hours. There is no obvious correlation among cases between frontal speed and temperature drop. The one case which moved the fastest did experience the largest temperature drops, but the case which shows the smallest drops has the second fastest movement.

The calculated convergence associated with each case is what should be expected. The maximum convergence in all cases occurs in the cold air, and extends into the warm air. The values of divergence and other kinematic quantities are two orders of magnitude greater than on synoptic scale. Although this results from the small grid interval chosen, it appears to be representative of the mechanisms in operation.

Vorticity has the poorest correlation with the fronts, and has no systematic pattern. On the average, cyclonic vorticity is found near the front with the exception of one area of anticyclonic vorticity in the March 23, 1965 case. Maximum values of cyclonic vorticity are at best weakly correlated with the small waves on the fronts. This is contrary to geostrophic

expectations and to the results of Petterssen and Austin (1942).
The scale of analysis must be an important factor, as Williams
(1962) found even weaker correlations in microscale vorticity
patterns.

The temperature field in each case is what should be expected.
The maximum gradients in the cold air occur within ten miles
of each front. The dilatation axes are generally parallel to
the isotherms in the frontal zones due to well organized wind
fields. The orientation of these axes is less favorable once
removed from the frontal zones.

The absolute magnitude of resultant deformation is the
most systematic kinematic quantity investigated. Large values
of deformation are characteristic of the frontal zones in each
case. A comparison of the divergence and deformation fields
indicates that deformation fields are both broader and more
intense in all cases.

The frontogenetical function has a maximum in the cold air
where the largest temperature gradients are located. In the
March 24, 1964 case the fields of convergence, deformation,
and temperature gradient are favorably coincident yielding
large value of frontogenesis throughout the frontal zone.
By comparison, it appears that this case is undergoing the
greatest frontogenesis at the time chosen. The other two cases
have isolated areas of large frontogenesis which are highly
correlated with the deformation fields.

We calculate huge rates of frontogenesis in all cases,
but find negligible change in frontal intensity as it moves
through the network. There are two possible models which might
account for this. First the front may propagate through the
air acting on different parcels. This would occur if it were
not a substantial surface. In this model, large values of
frontogenesis would be generated in advance of the front and
equally large values of frontolysis to the rear. We must
reject this model on the basis of results, which do not exhibit
large values of frontolysis behind the fronts.

The second possibility is that the front moves with the
air as a substantial surface but there is a balance between
mesoscale frontogenetical processes and turbulent frontolytical
processes. These frictional dissipative processes would have
to be of the same order to negate the huge rates of fronto-
genesis which we have computed. This model is the more appealing
of the two in light of the results. Diabatic effects must
naturally be important in any model of frontogenesis. It is
impossible to analytically calculate this process, but the
results of one case indicate that it may be of the same order
of magnitude as the frontogenetical function.

We have found that deformation fields are extremely
important in mesoscale frontogenesis. The general impression
is that these fields are characterized by large hyberbolic
streamline patterns which are evident on synoptic scale charts.

It is hoped that we have shown that this type of pattern is not a requirement in mesoscale analysis and that other types of flow can produce larger rates of deformation important to frontogenesis.

Investigation of Wind-Shift and Temperature Break

Plotkin (1965) showed that the wind-shift at a cold front
is a dual phenomenon whereby a directional wind-shift precedes
the temperature break, and a secondary surge in wind or vector
shift accompanies or immediately precedes the break. The peak
wind speed thus occurs at the beginning of the temperature
break and we find difluence in the zone of maximum temperature
gradient producing frontolysis. The timing in this case,
however, was crude because of inadequate time checks and instru-
mentation. Sanders (1966) investigated the March 23, 1965 case
in the Beta Network and was able to measure the temperature
break and wind-shift more precisely. His conclusions indicate
that maximum convergence occurs ahead of the break and extends
a small distance into the cold air, producing large rates of
frontogenesis. Elsewhere in the cold air there is divergence
and frontolysis on the average.

In the introduction, it was mentioned that some Meteoro-
logists use the wind-shift as the criterion for frontal location.
We choose the temperature break as the criterion in this paper,
because we find it less ambiguous as discussed above. We will
now investigate the relation between these two events in deter-
mining rates of frontogenesis. Because of the duality in the
wind-shift, we will refer to the initial shift in direction
as the wind-shift and the secondary surge as the vector shift.

Results

March 24 1964

The maximum nine-minute temperature drops figure 5b are
found during the first few hours. As the front progresses,
there appears to be a slight decrease in these drops and
possibly a slight increase as it is leaving the network. The
difference between the times of temperature break and wind-
shift figure 11a are indicated to nearest minute. The time of
temperature break was read from thermograph traces such as
figure 2 and the wind-shift, which in all cases was at least
22.5 degrees in one minute, was read from the continuous wind
records. The front has an average speed of nine knots and
average orientation of 250-070 degrees. The average difference
in time of the two events figure 11a is 1.54 minutes for 35
stations with usable records. There is an extremely good
correlation between this difference and the magnitude of the
nine-minute temperature drop figure 5b. The zero isoline
encompasses the maximum drops. As the time between the two
events decreases,there is a corresponding growth in the tempera-
ture drop.

The vector shift is generally coincident with the wind
shift at the stations in the northern half of the network,
producing large rates of frontogenesis. In the middle of the
network, the wind-shift outruns the temperature break and the
vector shift is weak producing small rates of frontogenesis. In
the southern half of the network the vector shift and wind-
shift are again coincident producing vigorous frontogenesis.

figure 11 (a) Difference in minutes between times of tempera-
ture break and wind-shift for March 24, 1964
case.

(b) March 23, 1965 case, same notation as in (a).

(c) April 24, 1965 case, same notation as in (a).

(a)

MARCH 24, 1964

(b)

MARCH 23, 1965

(c)

APRIL 24, 1965
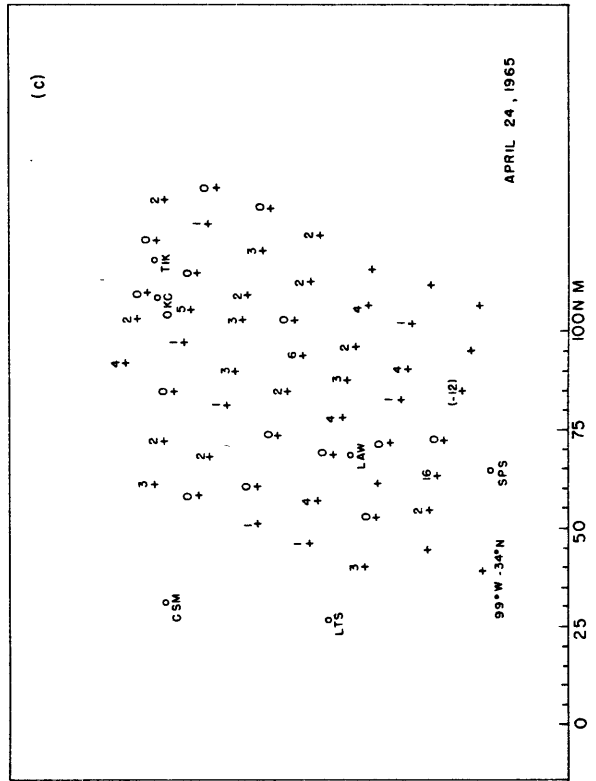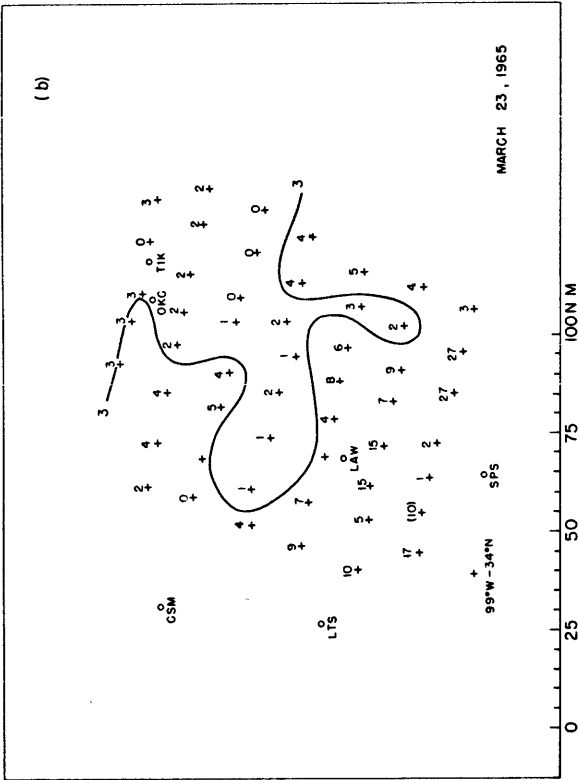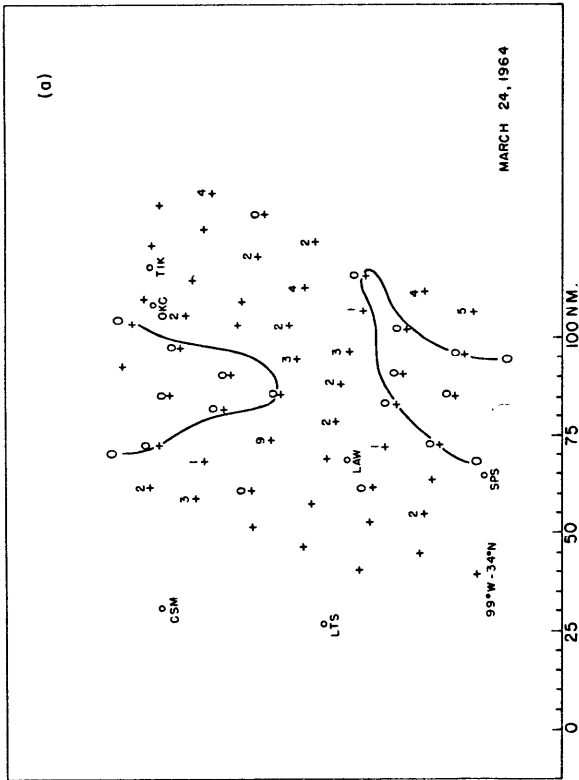
March 23 1965

The largest nine-minute temperature falls figure 7b

occurred in this case, which was previously investigated by

Sanders(1966). Maximum drops occur in the northern portion of

the network and are reduced by one half before leaving. The

front moves with an average velocity of 24 knots and has an

average orientation of 240-060 degrees. The difference

between shifts figure 11b indicates that the wind-shift

occurs increasingly ahead of the temperature break as the front

progresses,with a maximum value of twenty-seven minutes. The

large areas of simultaneous shifts are absent, and the average

difference for 51 stations is 4.86 minutes. The three minute

isoline encompasses the majority of the large nine-minute

temperature drops.

The vector shifts occur in the cold air at all stations

and are more vigorous to the north of the network. The front

is undergoing frontogenesis in the north and as it progresses

the vector shift decreases in magnitude. Normally the

largest values of convergence are associated with the direction-

al wind-shift and smaller values with the vector shift.

Because the vector shift is occurring in the cold air, it must

be the mechanism responsible for producing frontogenesis. As

the vector shift decreases, the turbulent scale processes

dominate and we have net frontolysis in the southern half of

the network.

April 24 1965

This case produced the smallest nine-minute temperature

drops. The front has an average speed of twelve knots and

average orientation of 230-050 degrees. The temperature

drop field figure 9b is not as well organized as the two previous

cases. Two possible reasons for this are the inequality of

solar radiation due to cloud conditions, and the outbreak of

thunderstorm activity in the southern half of the network.

There are indications of small increases in the nine-minute

temperature drops in the middle of the network. The difference

between shifts figure 11c shows a poorly organized pattern

with an average difference of 2.04 minutes for the 51 stations.

The vector shift is weak to the north, but increases in

magnitude as the front porgresses through the network. These

increases in velocity last only one to two minutes after which

the wind field becomes strongly difluent. In this case, it is

possible to examine the wind records and predict the general

magnitude of the nine-minute temperature drops. If the

thermograph traces figure 2 suffer from too large a time

constant, it is possible that near zero order temperature dis-

continuities do in fact exist in the atmosphere. Huge rates

of frontogenesis then could result from a vector shift occurring

in these regions.

Conclusions

We find a definite correlation between the rate of fronto-
genesis and the time difference between the temperature break
and the wind-shift. In areas where the two are coincident, huge
rates of frontogenesis occur because the area of largest
convergence is acting on the zone of maximum temperature gradient.
As the wind shift outruns the temperature break, advective
processes and frontogenesis produced by the vector shift
create the temperature drops. In near zero order temperature
discontinuities exist, the vector shifts may be capable of pro-
ducing huge rates of frontogenesis. When the vector shift
becomes weak, the weak mesoscale frontogenetical processes
are dominated by turbulent frontolytical process resulting in
net frontolysis.

In Plotkin's case (1965), the peak wind speed occurs in the
warm air, while it occurs in the cold air for all three cases
studied here. A model which might reconcile this, is as
follows. The peak wind speed originally is well within the cold
air, but propogates somewhat faster than the temperature
break. So long as it remains within the cold air we have
frontogenesis. When it reaches the frontal boundary or enters
the warm air we have frontolysis.

BIBLIOGRAPHY

Bergeron, T., 1928: Über die dreidimensional verknupfende
Wetteranalyse Geof. Pub. Vol. 5, No. 6.

Eliassen, A., 1959: On the Formation of Fronts in the
Atmosphere, The Rossby Memorial Volume Rockefeller
Inst. and Oxford University.

Petterssen, S., 1936: Contribution to the Theory of Fronto-
genesis, Geof. Pub. Vol.11, no. 6

Petterssen, S. and Austin, J. M. 1942: Fronts and Fronto-
genesis in Relation to Vorticity, Papers Phys.Ocean. Met.,
M. I. T. and W. H. O. I. Vol. 7, no. 2.

Petterssen, S., 1956: Weather Analysis and Forecasting
McGraw-Hill p. 189-213.

Plotkin, J., 1965: Detailed Analysis of an Intense Surface
Cold Front. M. S. Thesis, Dept. Meteor., M. I. T.

Sanders, F., 1966: Detailed Analysis of an Intense Surface
Cold Front. Presented to AMS meeting, Denver, Colorado,
25 January 1966.

Saucier, W. J., 1953: Horizontal Deformation in Atmospheric
Motion, Trans. An. Geo. Union Vol. 34, no.5.

Williams, D. T., 1962: A Report of the Kinematic Properties
of Certain Small-Scale Systems, National Severe Storms
Project, Report no. 11.